Наносистеми, наноматеріали, нанотехнології
Nanosistemi, Nanomateriali, Nanotehnologii
2022, т. 20, № 2, сс. 577–590

PACS numbers: 78.67.Ve, 81.07.Pr, 81.70.Pg, 82.35.Np, 87.19.xj, 87.64.Ee, 87.85.Rs

Magnetic-Liquid Nanosystems Fe_3O_4/PLA–PEG: Potential Applications in Cancer Thermotherapy

Quoc Thong Phan[1], Chi Thang Nguyen[2], and Huu Nguyen Luu[3]

[1]*University of Khanh Hoa,*
01, Nguyen Chanh, Nha Trang,
650000 Khanh Hoa, Vietnam
[2]*Nha Trang Institute of Technology Research and Application — VAST,*
02, Hung Vuong,
650000 Nha Trang, Vietnam
[3]*Ton Duc Thang University,*
19, Nguyen Huu Tho, Quan 7,
650000 Ho Chi Minh, Vietnam

In recent years, magnetic-liquid nanosystems (MNLs) have been of interest to biomedical applications. The Fe_3O_4/PLA–PEG MLNs with Fe_3O_4 magnetic nanoparticles' core coated by PLA–PEG copolymer are used based on their nontoxicity, biocompatibility, and ability to increase heat based on the alternating external magnetic field. The Fe_3O_4/PLA–PEG MLNs of poly(lactide)–polyethylene glycol (PLA–PEG) with PLA:PEG (3:1, w/w) component ratio were fabricated by ring-opening polymerization of lactide for preparation. In particular, the sample *in vitro* investigation achieved a high induction heating effect that indicates the applicability of the Fe_3O_4/PLA–PEG MLNs incorporated magnetic induction hyperthermia (MIH) treatment. From this work, we believe that Fe_3O_4/PLA–PEG MLNs exhibit great potential properties for biomedical applications.

В останні роки магнетні рідкі наносистеми (МРНс) представляють інтерес для біомедичних застосувань. МРНс Fe_3O_4/ПЛа–ПЕГ з магнетним ядром наночастинок Fe_3O_4, покритим сополімером полі(лактид)–поліетиленгліколь (ПЛа–ПЕГ), використовуються завдяки їхній нетоксичності, біосумісності та здатності збільшувати тепло на основі змінного зовнішнього магнетного поля. МРНс Fe_3O_4/ПЛа–ПЕГ зі співвідношенням компонентів ПЛа:ПЕГ (3:1, за вагою) були одержані шляхом кільцевої полімеризації лактиду для ліків. Зокрема, дослідження зразка у пробірці досягло високого індукційного нагрівального ефекту, що вказує на застосовність МРНс Fe_3O_4/ПЛа–ПЕГ, що включають лікування магнетно-індукційною гіпертермією (МІГ). З цієї роботи ми вважаємо, що МРНс Fe_3O_4/ПЛа–ПЕГ демонструють великі потенційні власти-

вості для біомедичних застосувань.

Key words: PLA–PEG copolymer, Fe_3O_4 nanoparticles, Fe_3O_4/PLA–PEG magnetic-liquid nanosystems, magnetic induction hyperthermia treatment.

Ключові слова: сополімер полі(лактид)–поліетиленгліколь, наночастинки Fe_3O_4, магнетні рідкі наносистеми Fe_3O_4/полі(лактид)–поліетиленґліколь, лікування магнетно-індукційною гіпертермією.

(Received 6 October, 2021; in revised form, 9 October, 2021)

1. INTRODUCTION

In recent years, magnetic nanoparticles have been studied with wide applications in the biomedical field, including detection, imaging, and therapeutic treatment, magnetic resonance imaging (MRI) contrast enhancement [1–5], as well as cancer hyperthermia [3]. However, the nanoparticles will be unstable and easily clumped or agglomerated, reducing dispersibility and biocompatibility, leading to them being easily eliminated [4–6]. Therefore, the surface functionalization of magnetic nanoparticles is necessary to improve the dispersion and some biochemical characteristics [7]. Typically, organic materials are used for functionalization purposes, and polymeric micelles themselves are considered multifunction materials for drug delivery and diagnostic imaging [1]. The copolymer of hydrophilic and hydrophobic self-assembly separate chains forms a nanostructure that can produce supramolecular core–shell structures (10–100 nm) dispersed in water to form magnetic-liquid nanosystems (MLNs). The hydrophobic core of the micelles can carry hydrophobic agents, while the hydrophobic shell stabilizes the nanoparticles in water [8].

Among the MLNs recently studied, Fe_3O_4 nanoparticles incorporated in the polymer micelle have been reported as a potential candidate [9, 10]. It demonstrated the ability to improve the biocompatibility and extent the blood circulation time [11]. Typically, the Fe_3O_4 nanoparticles incorporated in the polymer micelle were synthesized by microemulsion, sol–gel, hydrothermal, thermal decomposition method, *etc.* [12–15].

On the other hand, magnetic nanoparticles need to be coated to increase biocompatibility, reduce toxicity and increase blood circulation [3]. The local killing ability of magnetic nanoparticles based on alternating external magnetic fields has been studied and applied in thermotherapy to kill cancer cells and tumours due to its ease of implementation, low cost, and reduced complication [18]. Recent studies have shown that magnetic nanoparticles are considered an

effective, versatile tool and have great applicability in the biomedical field, including the ability to kill cancer cells by thermotherapy [10].

In this work, we synthesized the MLNs consisting of Fe_3O_4 nanoparticles by the coprecipitation method [16]. Fe_3O_4 nanoparticles coated by a copolymer of co(lactide)–polyethylene glycol (PLA–PEG) and then dispersed in water to form Fe_3O_4/PLA–PEG MLNs. In which, PEG was used as a hydrophilic shell and PGA as a hydrophobic core. The balance between hydrophobic core–hydrophilic shell in water creates the spontaneous formation of nanoparticles [6, 17]. The Fe_3O_4 nanoparticles before and after coating PLA–PEG copolymer is compared. Thereby research the effect of PLA–PEG copolymer coating on the saturation of Fe_3O_4 nanoparticles. On the other hand, *in vivo* investigations to kill cancer cells by MIH effect were also performed.

The structure and characteristics of the system were investigated by FE-SEM (field emission scanning electron microscopy), TEM (transmission electron microscopy), and (XRD) x-ray diffraction. The copolymer coverage of the nanoparticles is displayed through FTIR (Fourier transform infrared spectroscopy) measurement results. The mass contributions of the components were analysed by the TGA (thermal gravity analysis) measurement. The heating efficiency of the functionalized nanoparticles was demonstrated through MIH (magnetic induction hyperthermia) study.

2. MATERIAL AND METHODS

2.1. Synthesis, Characterization, and Structure of Magnetic Nanoparticles

Monolactide acid (LA), polyethylene glycol-2000 (PEG 2000), tin (II) 2-ethylhexanoate purchased from Sigma (St. Louis, MO, USA); and $FeCl_3$, $FeCl_{2\cdot4}H_2O$, NH_4OH, toluene, diclomethan (DCM, $C_2H_2Cl_2$), methanol (CH_3OH), ethanol (C_2H_5OH) purchased from Merck (Germany). The water was used in the experiment is double distilled water.

PLA–PEG copolymer with PLA:PEG ratio at 3:1 (by weight) was prepared using ring-opening polymerization, in which the reaction occurred between lactic monomer and polyethylene glycol (PEG) in the presence of tin (II) 2-ethylhexanoate catalyst [19]. The PLA–PEG copolymer was dissolved in DCM (1 mg/ml) and stirred for 24 hours. Then, H_2O was added to form the liquid mixture, stirring to disperse this mixture for 24 hours. Finally, the PLA–PEG copolymer dispersed in H_2O (1 mg/ml) was obtained from the evacuation of DCM solvent.

The coprecipitation method [20] was used to synthesis Fe_3O_4 nanoparticles according to the following equation:

$$2Fe^{3+} + Fe^{2+} + 8OH^- \rightarrow Fe_3O_4 + 4H_2O.$$

The surface of Fe_3O_4 nanoparticles was functionalized by PLA–PEG copolymer into water. The amount of Fe_3O_4 nanoparticles dispersed in water was first determined, then slowly dropped into PLA–PEG copolymer solution and stirred for 24 hours to obtain Fe_3O_4/PLA–PEG nanoparticles.

XRD (Empyrean, PANalytical, Netherland) was used to determine the crystal structure of nanoparticles, FE-SEM (JEOL JSM-4600F, US) and TEM (JEOL, JEM-1010) microscopes were used for size and size distribution characterization. The dynamic light scattering (DLS) measurements (Zetasizer-Nano ZS, Malvern, UK) was adopted to estimate the Fe_3O_4/PLA–PEG nanoparticle hydrodynamic diameter. The chemical bonds were observed by FTIR spectroscopy (Shimadzu FT–IR Prestige-21, Japan); meanwhile, the mass contribution of PLA–PEG was identified by Thermal Gravity Analysis (TGA, Shimadzu DTG-60H, Japan). Hysteresis loops at room temperature up to 11 kOe and M–T curves were measured by a homemade vibrating sample magnetometer (VSM).

2.2. Preparation for Magnetic Inductive Heating (MIH)

Experiments to determine the MIH effect of the Fe_3O_4/PLA–PEG MLNs were carried out on two pieces of equipment to measure specific absorption rate (SAR):

$$\mathrm{SAR} = C_1(m_1/m_{cs})\frac{\partial T}{\partial t}, \tag{1}$$

where C_1 is the liquid heat capacity (4.186 J/(g·°C) for water), m_1 and m_{cs} are correspondingly masses of liquid and MLNs; $\partial T/\partial t$—the initial rate of temperature increase.

Low-field equipment based on an RDO generator of 5 kW was used to measure the heating curves of Fe_3O_4/PLA–PEG MLNs in the field amplitude smaller than 100 Oe and frequency below 250 kHz, and this system was used for the controlled drug release experiment. The second MIH equipment used in an Ambrell Easyheat LI 3542 system of 4.2 kW generator provided field at 310 kHz with field amplitudes varying from 200 to 800 Oe.

Samples of Fe_3O_4/PLA–PEG MLNs with concentrations of 1 and 3 mg/ml were measured for temperature change with distilled water used as the sole suspension solvent.

2.3. *In vivo* Cancer Cells' Treatment

In this experiment, a magnetic field of 60 Oe, frequency of 310 kHz, the concentration of Fe_3O_4/PLA–PEG MLNs 2 mg/ml was used to heat treatment to kill cancer cells.

In an *in vitro* cultured cancer cell model, $5 \cdot 10^6$ Sarcoma 180 cells were inoculated with Fe_3O_4/PLA–PEG MLNs (2 mg/ml). After heat treatment for 60 minutes with an alternating external magnetic field of 70 Oe, frequency 178 kHz, the cell samples were stained with blue trypan to determine the percentage of dead cells.

3. RESULT AND DISCUSSION

3.1. Fabrication and Characterization

The diagram in Fig. 1 describes the coating process of the PLA–PEG micelle around the Fe_3O_4 nanoparticle core, forming a Fe_3O_4/PLA–PEG core–shell structure system with hydrophobic properties.

The XRD diagram (Fig. 2) shows that six peaks of both Fe_3O_4 and Fe_3O_4/PLA–PEG samples (Fig. 2) are clearly defined. The characteristic diffraction peaks of the spinel structure: (200), (311), (400), (422), (511), and (400) [16] on the XRD diagram were independent. This result suggests that the formation of Fe_3O_4/PLA–PEG compositional nanoparticles does not affect the Fe_3O_4 crystal structure, which can lead to the conservation of the magnetic properties of the system. It will be discussed in the next section.

The average size of the core nanocrystal, d_c, estimated from XRD profile *via* Scherrer formula (Eq. (2)) [21] was around 15 nm, which is consistent with results shown in TEM images (Fig. 3).

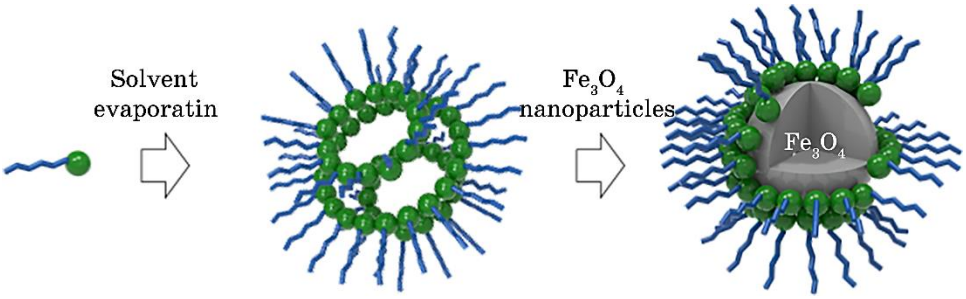

Fig. 1. Schematic illustration of fabrication route of Fe_3O_4/PLA–PEG nanocarriers.

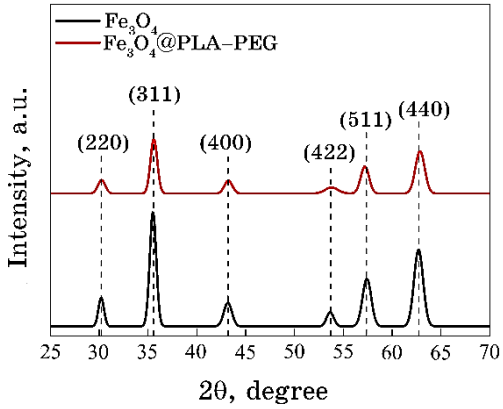

Fig. 2. XRD diagrams of Fe_3O_4 and Fe_3O_4/PLA–PEG.

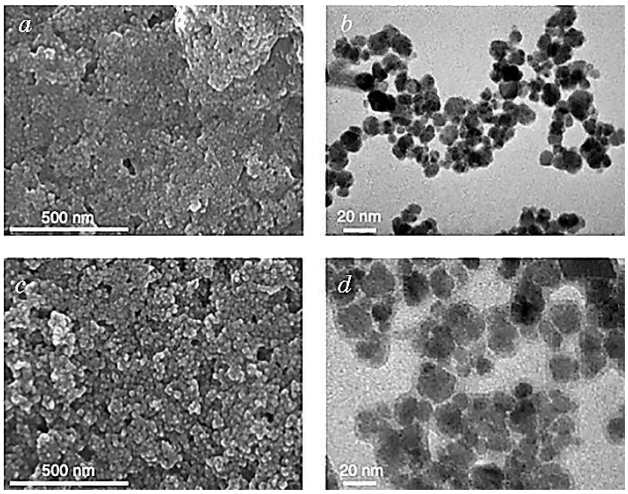

Fig. 3. SEM and TEM images of nanoparticles: Fe_3O_4 (*a*, *b*), Fe_3O_4/PLA–PEG (*c*, *d*).

$$D = \frac{k\lambda}{\beta \cos \theta_B}, \tag{2}$$

where D is average crystal diameter; $k \cong 0.9$ is a constant value related to shape particle; λ is electromagnetic radiation wavelength; θ_B is Bragg diffraction angle; β is the line broadening at the full-width-half-maximum intensity (FWHM) subtracted the instrumental line broadening, in radians.

TEM images of Fe_3O_4, Fe_3O_4/PLA–PEG samples are displayed in Fig. 3 showing that each spherical nanoparticle has a single core.

The functionalized Fe_3O_4/PLA–PEG nanoparticles are fairly uniform with an average diameter of *ca.* 20 nm (Fig. 3, *d*) and larger than that of the Fe_3O_4 nanoparticles (*ca.* 15 nm as shown in Fig. 3, *b*). Figure 3, *d* clearly points out that the functionalized Fe_3O_4/PLA–PEG nanoparticles have core–shell structures. For such a core–shell formation, it is assumed that the Fe_3O_4 nanoparticles attract PLA component to form a strong binding on the core particle surface after penetrated the centre of PLA–PEG nanoparticles (of *ca.* 50 nm in size [16]) so that the outmost size of the copolymer particles become reduced to *ca.* 20 nm.

3.2. FTIR Spectra

The FTIR spectra of the Fe_3O_4 and Fe_3O_4/PLA–PEG nanoparticles are shown in Fig. 4. The shift was found from the peak at 632 cm^{-1} of the Fe_3O_4 nanoparticles spectrum (by the stretching of Fe–O bond) to the peak at 628 cm^{-1} in the Fe_3O_4/PLA–PEG spectrum. It demonstrates that the PLA–PEG coating has contributed to Fe_3O_4 particles. Moreover, the appearance of peak 1348 cm^{-1} on the FTIR spectrum of Fe_3O_4/PLA–PEG nanoparticles also indicates the copolymer coating on the ferromagnetic nanoparticles [22].

3.3. Effect of PLA–PEG to Saturation Magnetization of Fe_3O_4/PLA–PEG Nanoparticles

In this section, the saturation magnetization M_s of Fe_3O_4/PLA–PEG nanoparticles was examined in the different Fe_3O_4 nanoparticles concentration (from 1 mg/ml to 5 mg/ml), while the concentration of copolymer PLA–PEG remained unchanged (0.3 mg/ml).

Figure 5 shows the magnetic hysteresis curve of Fe_3O_4 nanoparticles, coated by various PLA–PEG mass ratios and measured at room temperature. The saturation magnetization values M_s were measured and the nonmagnetic polymer mass M_s^{nom} were calculated based on the nominal percentage and presented in Table 1.

The increase of saturation magnetization is observed with the increase of Fe_3O_4 composition (from sample No. 1 to sample No. 5). It is primarily due to the functionalization of the coated samples. A significant increase (up to 10%) of magnetization is evidenced. In other words, our experiment indicated that the coating with an appropriately biodegradable polymer (PLA–PEG) might somehow restore the magnetization reduction of the core Fe_3O_4 nanoparticles that was resulted during nanoparticle synthesis in general and their coprecipitation synthesis [23].

On the other hand, the highest saturation magnetization accom-

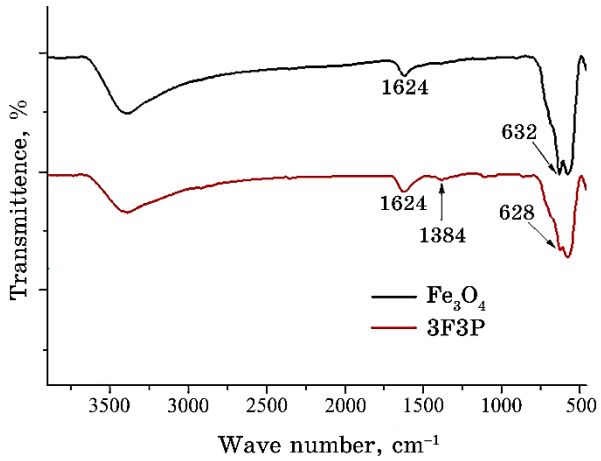

Fig. 4. FTIR spectra of nanoparticles Fe_3O_4, Fe_3O_4/PLA–PEG.

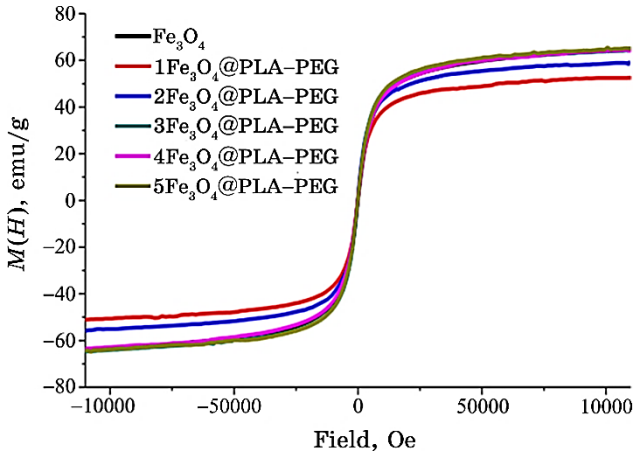

Fig. 5. Magnetic hysteresis curves of Fe_3O_4 nanoparticles functionalized by PLA–PEG of various concentrations.

panying the highest stability in the No. 3 sample suggests that dispersion stability could be a crucial cause for high magnetization restoration.

The nanoparticle sample of Fe_3O_4 and Fe_3O_4/PLA–PEG were analysed by TGA (diagrams are shown in Fig. 6) to estimate the mass contribution of nonmagnetic coating materials PLA–PGE in the experimental samples.

Table 2 summarizes the TGA-determined mass percentage m^{ex} along with the nominal mass m^{nom} for the coated samples. The data indicate that the mass percentages determined experimentally by

TABLE 1. Saturation magnetization M_s and M_s^{non} of Fe_3O_4 and Fe_3O_4/PLA–PEG.

Sample	Component		Fe_3O_4, %	M_s, emu/g	M_s^{nom}, emu/g
	Fe_3O_4, mg	PLA–PEG, mg			
Fe_3O_4	1	0	100	64.4	64.4
No.1	1	0.3	79.6	53	68.9
No.2	2	0.3	87	59.2	68.1
No.3	3	0.3	90.9	64.5	71
No.4	4	0.3	93	64.2	69
No.5	5	0.3	94.4	65.1	68.9

TABLE 2. Compare the mass percent of PLA–PEG experimentally determined TGA with the nominal value.

Sample	Component		$m_{Fe_3O_4}$	m^{nom}	m^{ex}
	Fe_3O_4, mg	PLA–PEG, mg			
Fe_3O_4	Fe_3O_4	0	100	0	0
No.3	3	0.3	90.9	91	13.5
No.5	5	0.3	94.34	5.66	5.667

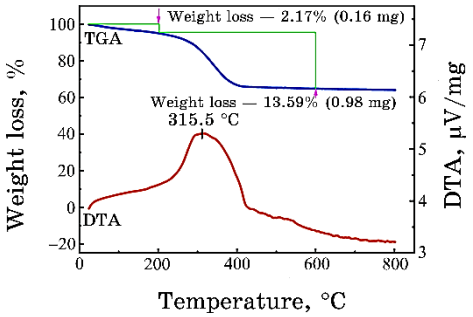

Fig. 6. TGA and DTA diagrams of Fe_3O_4@PLA–PEG.

TGA are consistent with those used in a nominal composition. This observation is consistent with that reported by Y. Piceiro-Redondo *et al.* [23].

The Fe_3O_4/PLA–PEG nanoparticles exhibit higher dispersion stability than Fe_3O_4. This result is significant in opening up many new applications for Fe_3O_4 nanoparticles in biomedical fields such as hyperthermia treatment, magnetic resonance imaging (MRI), and studying the effects of physical mechanisms on their magnetization saturation.

3.4. MIH Studies

As introduced, the heating efficiency of the functionalized nanoparticles, Fe_3O_4/PLA–PEG, after dispersing in water at concentrations of 1 and 3 mg/ml, was studied using MIH methods. The temperatures *vs.* time curves were recorded for different AC fields.

The heating curves measured with AC field amplitude varying from 200 to 800 Oe and at a constant frequency of 310 kHz are depicted in Fig. 7. As can be seen in this figure, the heating rate also increases with increasing field amplitude, and the final temperature of the medium rises to 42°C after 5 min and maybe rises to 55–60°C after 15 min magnetic inductive heating at a frequency of 310 kHz and AC fields of 800 Oe for the Fe_3O_4/PLA–PEG (approximately).

This result clearly shows that the therapeutic window for hyperthermia therapy, 40–45°C, can be easily reached within a few minutes by modifying the AC field amplitude during the treatment.

Another way, the heating efficiency or SAR for the Fe_3O_4/PLA–PEG sample with two different concentrations of 1 and 3 mg/ml were have calculated to get a better insight into the hyperthermia effect of the Fe_3O_4/PLA–PEG nanoparticles.

As can be observed, the SAR values obtained for the Fe_3O_4/PLA–PEG sample is achieved high efficiency of induction heating, especially at 1 mg/ml, reaching a maximum value of 228 W/g. This SAR value is comparable to what has been reported in the literature [24–26]. When the concentration increase to 3 mg/ml, the SAR increases not too high and reaches only about 174 W/g. This deterioration of the SAR can be related to particle aggregation with increasing concentration of MNPs, which tends to restrict the heating efficiency of the Fe_3O_4/PLA–PEG nanoparticles [23, 27].

Therefore, as can be seen from these results, the heating efficien-

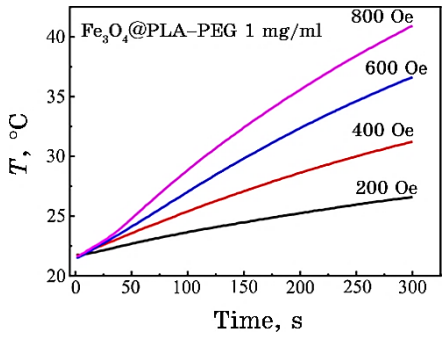

Fig. 7. Heating curves were taken at a frequency of 310 kHz and AC fields of 200, 400, 600, and 800 Oe for Fe_3O_4/PLA–PEG specimens of 1 mg/ml concentration.

TABLE 3. Comparison saturation magnetization of Fe_3O_4 nanoparticles measured before and after subtraction of PLA–PEG coating mass.

Sample	m_{sample}, μg	$M_s^{as\text{-}me}$, emu/g	M_s^{nom}, emu/g	M_s^{ex}, emu/g
Fe_3O_4	10.5	64.4	64.4	64.4
No.3	13.8	64.5	71	74.5

TABLE 4. SAR of Fe_3O_4/PLA–PEG samples measured at 310 kHz, and 1 mg/ml.

H, Oe	m_{H_2O}, g	m_{sample}, g	SAR, W/g
200	1.00	0.001	94
400	1.00	0.001	152
600	1.00	0.001	202
800	1.00	0.001	228

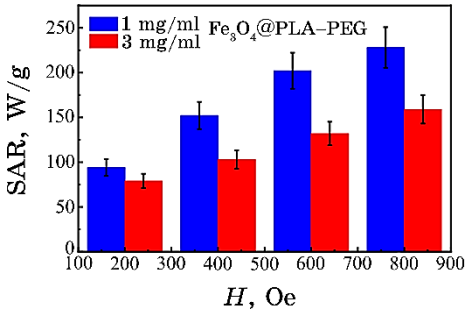

Fig. 8. SAR values for the Fe_3O_4/PLA–PEG nanoparticles, with 1 and 3 mg/ml, were obtained at different field amplitudes, 200–800 Oe and 310 kHz.

cy of Fe_3O_4/PLA–PEG is still remarkable even at the 3 mg/ml concentration, and they can be effectively used for hyperthermia treatment.

3.5. Kill Cancer Cells by MIH Using Fe_3O_4/PLA–PEG MLNS

Some previous research results [26] showed that using an alternating external magnetic field to heat the magnetic nanoparticles locally can damage and directly kill cancer cells. The thermotherapy method using Fe_3O_4/PLA–PEG MLNs shows that it can kill cancer cells, typically Sarcoma 180 cells.

In this experiment, we chose the Fe_3O_4/PLA–PEG MLNs with the concentration of 2 mg/ml, the magnetic field of 70 Oe, the frequen-

cy of 178 kHz to ensure that the temperature is in the thermotherapy region 42–52°C, and the Sarcoma 180 cancer cell line were used in this experiment. The results are presented in Table 5 and Fig. 9.

Research results show that Fe_3O_4/PLA–PEG nanoparticles have the ability to kill cancer cells based on local heating ability on alternating external magnetic fields.

The results of Table 5 show that cells continued to die when stopping the use of thermotherapy. At 60 minutes after stopping treatment, dead cells (green cells) achieve 61.4%.

On the other hand, the results in Table 5 and Fig. 9 show that, after the end of heating, Fe_3O_4/PLA–PEG nanoparticles are still capable of affecting and killing cells. Fe_3O_4 nanoparticles coated with PLA–PEG copolymer will help increase blood circulation, increase biocompatibility.

The saturation magnetic of core Fe_3O_4 nanoparticles tend to increase due to the impact of the nonmagnetic PLA–PEG shell on the surface of Fe_3O_4 nanoparticles.

These results open the possibility of applying Fe_3O_4/PLA–PEG MLNs to kill cancer cells and tumours by thermotherapy and in the biomedical field.

TABLE 5. Cell killing results by MIH (70 Oe, 178 kHz) using Fe_3O_4/PLA–PEG MLNs (2 mg/ml) with time of treatment of 45 min and 60 min.

Percentage of dead cells at time points after the end of the thermotherapy (%)		0′	10′	20′	30′	60′
Times of thermotherapy (45′)	Sample experiment	18.0	30.9	36.1	41.3	50.0
	Control	6.0	7.4	8.3	8.7	9.8
Times of thermotherapy (60′)	Sample experiment	23.1	37.8	50.7	56.3	61.4
	Control	6.9	7.5	7.0	7.3	8.6

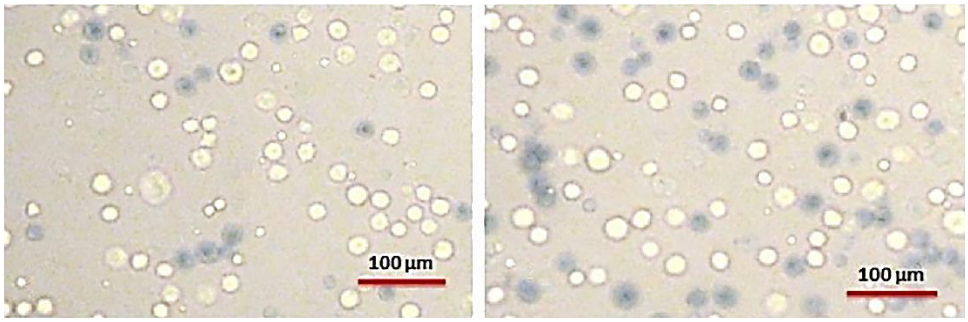

a *b*

Fig. 9. Sarcoma cells 180 at times: 0 min (*a*) and 60 min (*b*).

4. CONCLUSION

This study successfully synthesized Fe_3O_4 nanoparticles and functionalized them by PLA–PEG to form single-core Fe_3O_4/PLA–PEG core–shell nanoparticles. Besides, the coating layer helped improve the magnetic properties of the magnetic nanoparticles, including the higher saturation magnetization and lost power. The saturation magnetization of Fe_3O_4 nanoparticles after being functionalized is higher than that of uncoated Fe_3O_4 nanoparticles. Fe_3O_4/PLA–PEG MLNs have the ability to increase local heat based on alternating external magnetic fields, applied in thermotherapy to kill cancer cells and tumours. These results suggest the enormous potential of the Fe_3O_4/PLA–PEG MLNs in biomedical fields, especially in cancer treatment.

REFERENCES

1. L. Zhang, H. Xue, C. Gao, L. Carr, J. Wang, B. Chu, and J. Shaoyi, *Biomat.*, **31**, Iss. 25: 6582 (2010); https://doi.org/10.1016/j.biomaterials.2010.05.018
2. K. Kluchova, R. Zboril, J. Tucek, M. Pecova, L. Zajoncova, I. Safarik et al., *Biomat.*, **30**, Iss. 15: 2855 (2009); https://doi.org/10.1016/j.biomaterials.2009.02.023
3. A. J. Giustini, A. A. Petryk, S. M. Cassim, F. A. Tate, I. Baker, and P. J. Hoopes, *Nano Life*, **1**, No. 01n02: 17 (2010); https://dx.doi.org/10.1142%2FS1793984410000067
4. T. Reza and S. Negar, *Int. J. Biol. Macromol.*, **120**, Pt B: 2313 (2018); https://doi.org/10.1016/j.ijbiomac.2018.08.168
5. Y. Lu, E. Zhang, J. Yang, and Z. Cao, *Nano Res.*, **11**, No. 10: 4985 (2018); https://dx.doi.org/10.1007%2Fs12274-018-2152-3
6. S. Kim, Y. Shi, J. Y. Kim, K. Park, and J. X. Cheng, *Expert. Opin. Drug Deliv.*, **7**, No. 1: 49 (2010); https://doi.org/10.1517/17425240903380446
7. M. D. Shultz, J. U. Reveles, S. N. Khanna, and E. E. Carpenter, *J. Am. Chem. Soc.*, **129**, No. 7: 2482 (2007); https://doi.org/10.1021/ja0651963
8. V. P. Torchilin et al., *Adv. Drug Deliv.*, **54**, No. 2: 235 (2002); https://doi.org/10.1016/s0169-409x(02)00019-4
9. T. Prabhakaran and J. Hemalatha, *Mat. Chem. Phys.*, **137**, No. 3: 781 (2013); https://doi.org/10.1016/j.matchemphys.2012.09.064
10. Z. Bakhtiary, A. A. Saei, M. J. Hajipour, M. Raoufi, O. Vermesh, and M. Mahmoudi, *Nanomed.: Nanotech., Biol. Med.*, **12**, No. 2: 287 (2016); https://doi.org/10.1016/j.nano.2015.10.019
11. V. P. Torchilin et al., *Adv. Drug Deliv. Rev.*, **58**, No. 14: 1532 (2006); https://doi.org/10.1016/j.addr.2006.09.009
12. A. L. Oppegard, F. J. Darnell, and H. C. Miller, *J. Appl. Phys.*, **32**, Iss. 3: S184 (1961); https://doi.org/10.1063/1.2000393
13. B. L. Cushing, L. Vladimir, V. L. Kolesnichenko, and C. J. O'Connor, *Chem. Rev.*, **104**, No. 9: 3893 (2004); https://doi.org/10.1021/cr030027b

14. D. Zhao, X. Wu, H. Guan, and E. Han, *J. Sup. Flu.*, **42**, Iss. 2: 226 (2007); http://dx.doi.org/10.1016%2Fj.supflu.2007.03.004
15. J. Park, J. Joo, S. G. Kwon, Y. Jang, and T. Hyeon, *Ang. Chem. Int. Edi.*, **46**, No. 25: 4630 (2007); https://doi.org/10.1002/anie.200603148
16. S. Laurent, D. Forge, M. Port, A. Roch, C. Robic, L. V. Elst, and R. N. Muller, *Chem. Rev.*, **108**, No. 6: 2064 (2008); https://doi.org/10.1021/cr068445e
17. D. Attwood, C. Booth, S. G. Yeates, C. Chaibundit, and N. M. P. S. Ricardo, *Int. J. Pharm.*, **345**, Nos. 1–2: 35 (2007); https://doi.org/10.1016/j.ijpharm.2007.07.039
18. M. Salloum, R. H. Ma, D. Weeks, and L. Zhu, *Int. J. Hyp.*, **24**, No. 4: 337 (2008); https://doi.org/10.1080/02656730801907937
19. Q. T. Phan, M. H. Le, T. T. H. Le, T. H. H. Tran, P. N. Xuan, and P. T. Ha, *Int. J. Pharm.*, **506**, Nos. 1–2: 32 (2016); https://doi.org/10.1016/j.ijpharm.2016.05.003
20. T. Shen, R. Weissleder, M. Papisov, A. Bogdanov, and T. J. Brady, *Magn. Reson. Med.*, **29**, No. 5: 559 (1993); https://doi.org/10.1002/mrm.1910290504
21. F. A. S. da Silva, E. E. G. Rojas, and M. F. de Campos, *Mat. Sci. Engin.*, **820**, Spec. Iss.: 373 (2015); https://doi.org/10.4028/www.scientific.net/MSF.820.373
22. I. Hilger and W. A. Kaiser, *Biol. Med.*, **7**, No. 9: 1443 (2012); https://doi.org/10.2217/nnm.12.112
23. Y. Piceiro-Redondo et al., *Nanoscale Res. Lett.*, **6**, No. 1: 383 (2011); https://doi.org/10.1186/1556-276x-6-383
24. A. E. Deatsch and B. A. Evans, *J. Magn. Magn. Mater.*, **354**: 163 (2014); https://ui.adsabs.harvard.edu/link_gateway/2014JMMM..354..163D/doi:10.1016/j.jmmm.2013.11.006
25. M. A. Gonzalez-Fernandez, T. E. Torres et al., *J. Solid State Chem.*, **182**: 2779 (2009); http://dx.doi.org/10.1016/j.jssc.2009.07.047
26. H. Parmar, I. S. Smolkova, N. E. Kazantseva, V. Babayan, P. Smolka, R. Moučka et al., *Procedia Eng.*, **102**: 527 (2015); http://dx.doi.org/10.1016/j.proeng.2015.01.205
27. E. Lima Jr., E. de Biasi, M. V. Mansilla, M. E. Saleta, M. Granada, H. E. Troiani et al., *J. Phys. D: Appl. Phys.*, **46**: 045002 (2013); https://doi.org/10.1088/0022-3727/46/4/045002